Journal of Materials Chemistry A

Accepted Manuscript

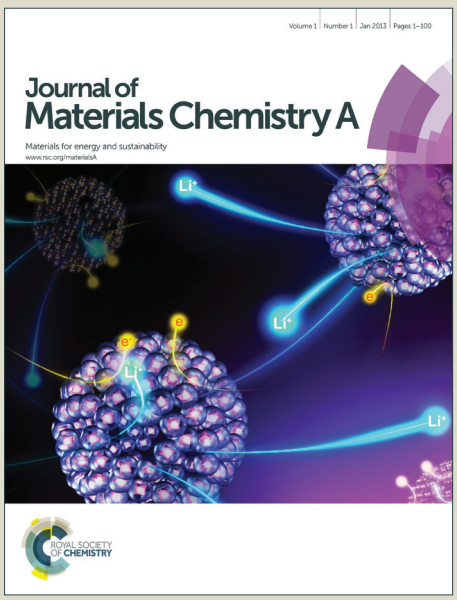

ROYAL SOCIETY OF CHEMISTRY

www.rsc.org/materialsA

Cite this: DOI: 10.1039/c0xx00000x

www.rsc.org/xxxxxx

ARTICLE TYPE

Selective Laser Sintering of TiO_2 Nanoparticles Film on Plastic Conductive Substrate for Highly Efficient Flexible Dye-sensitized Solar Cell Application

Liqun Ming,[†a] Huan Yang,[†a] Wenjun Zhang,[a] Xianwei Zeng,[a] Dehua Xiong,[a] Zhen Xu,[a] Huan Wang,[a] Wei Chen,[*a] Xiaobao Xu,[a] Mingkui Wang,[*a] Jun Duan,[*a] Yi-Bing Cheng,[a,b] Jie Zhang,[b] Qiaoliang Bao,[b] Zhanhua Wei,[c] Shihe Yang[c]

Received (in XXX, XXX) Xth XXXXXXXXX 20XX, Accepted Xth XXXXXXXXX 20XX
DOI: 10.1039/b000000x

In this paper, we report a novel selective laser sintering of TiO_2 nanoparticles (Degussa P25) film on plastic conductive substrate for highly efficient flexible dye-sensitized solar cell (DSC) application. The so-called "selective sintering" means that, the absorbed laser energy can effectively promote the electrical contacts between the TiO_2 nanoparticles, but does not cause damage to the plastic conductive substrate. The choice on the near-infrared (wavelength = 1064 nm) laser source is critical for the effectiveness of the laser sintering. The laser sintering technology can effectively decrease electron transport resistance and increase recombination resistance of the TiO_2 nanoparticles film characterized by electrochemical impedance spectroscopy and transient photovoltage/photocurrent decays measurements, resulting in much improved charge collection efficiency. Thus, compared to the reference sample, the laser sintered film has achieved an improved short-circuit current density from 9.2 to 10.4 mA cm^{-2}, fill factor from 0.71 to 0.77, and solar conversion efficiency from 4.5% to 5.7%.The fast and effective selective laser sintering technique has great potential to be integrated into scalable roll-to-roll manufacture of highly efficient flexible DSC.

Introduction

Flexible manufacturing of thin film solar cells is an important trend in today's photovoltaic market. Many innovation companies, *e.g.* G24 Innovations in UK, United Solar, Nanosolar, First Solar in the U.S., *etc*., have engaged in the competitions in order to realize large-scale industrialization of thin film solar cells on flexible metal foils or plastic conductive substrates.[1-4] In comparison to conventional rigid devices, flexible solar cells possess the following advantages: (1) their light weight and flexible features make them more suitable as portable power sources; (2) they are easily adapted to the complex surfaces, such as diverse building roofs and curtain walls, facilitating the future "Building Integrated Photovoltaics" applications; (3) their compatibility with roll-to-roll manufacture fashion further strengthen the low-cost advantage, largely shortening the energy payback time.[1]

Dye-sensitized solar cell (DSC), as one of the most promising next generation photovoltaic technologies, its flexible manufacturing has also attracted intensive attention from both academic and industrial researchers.[5, 6] Flexible substrates could be metal foils/meshes or conductive plastic films, such as indium tin oxide (ITO)-coated polyethylene terephthalate (PET) or ITO-coated polyethylene naphthalate (PEN). Metal foils or meshes have their own advantages for flexible DSC applications. The research in this field recently has gained considerable progresses.[7-11] However, the nontransparent metallic substrates require back side illumination, the undesired light absorption by the counter electrode and the electrolyte will always constitute limitation factors for this kind solar cells. In this work, we focus on the flexible DSCs on conductive plastic substrates. The current efficiency records for plastic substrates based flexible DSCs are about 7-8%, relatively lower than 11-12% of the conventional DSCs on rigid FTO glasses.[12-13] Such an efficiency gap mostly arises from elimination of the high temperature (450-550 °C) sintering procedure for TiO_2 nanoparticles film, which can be done for film deposited on FTO glasses but cannot on plastic substrates. The widely used ITO-PET or ITO-PEN plastic substrates can only endure thermal treatment below 120 or 150 °C. Within such a low temperature range, how to improve the necessary inter-nanoparticles physical/electrical contacts and therefore the effective charge collection capability for the photo-injected electrons, is of great significance for the cell performance.[14, 15] Up to now, though various low temperature techniques have been explored, including compression,[16] UV-

ozone treatment,[17] microwave sintering,[18] chemical sintering,[19, 20] and lift-off/transfer method,[21] *etc*., a facile and effective technique applicable to industrial production still remains as great challenge.

Cold isostatic press method was invented by prof. Yi-Bing Cheng,[22, 23] one of the co-authors of this paper, to prepare high uniform and robust TiO_2 nanoparticles films on plastic conductive substrates. The technology has been well reproduced in our lab. In this paper, on the basis of the decent benchmark cell prepared by cold isostatic press, we further introduced a novel selective laser (wavelength = 1064 nm) sintering technique to post-treat TiO_2 nanoparticles film on plastic conductive substrate. The fast laser treatment allows sufficient sintering of binder free TiO_2 nanoparticles film without damage to the ITO-PEN substrate. Remarkable efficiency of 5.7% has been finally achieved. It is the first time the near-infrared (IR) laser has been introduced to fabricate flexible DSC, different from previous reports mostly with UV laser.[24-26] In comparison to recently reported work by using near-IR lamp to fast sinter TiO_2 film on Ti foil,[27] the laser spectrum is nearly single wavelength; therefore, the reaction of laser beam on different materials will have more definite modes, which is very important for the selectivity of energy absorption by the TiO_2 layer and the ITO/PEN layer. Besides, the laser sintering effect on the TiO_2 film and the inherent relation with the performance of the solar cell device have been studied in detail.

Experimental Section

Preparation of TiO_2 films and flexible DSCs

The TiO_2 film was prepared on an cold isostatic press according to the literatures.[22, 23] Typically, a binder free paste consisting of 3.0 g TiO_2 nanoparticles (Degussa, P25) in 7.0 g ethanol was prepared by ball-milling at rotating speed of 350 rpm for 4 hrs. Then, the paste was processed into uniform film by a doctor blade technique on ITO-PEN substrate (14 Ω cm^{-2}, Peccell Technologies, Inc., Japan). Cold isostatic compression was carried out at the oil pressure of 200 MPa for 5 min. After that, robust TiO_2 film with good adhesion to the substrate was achieved. The film thickness was controlled at 13 μm.

The pressed film was then treated by the selective laser sintering on a computer controlled laser system with 1064 nm laser source, as schematically shown in Figure 1a. The TiO_2 film was placed on top of the 3-dimensional working table. The laser power (P) was set at 8 W. The focus of laser beam was set 14 mm above the TiO_2 film. The effective irradiation area of laser beam on the TiO_2 film surface was a circular spot with the diameter (d) of 368 μm, as shown in Figure 1b. The energy density (H) for the laser beam reaching the TiO_2 film surface was estimated to be 52 J cm^{-2}, according to the equation of $H = P/(V \times d)$.[26] The scanning trace was shown in Figure 1c: by a reciprocating motion with the repeating length of at least 6 mm and the scan-lines interval of 250 μm, a designed pattern of laser sintered film could be obtained. The scanning rate (V) was set at 30 mm $second^{-1}$. In such a scanning way, it requires only 5 seconds to finish a size of 6 × 6 mm^2 square pattern sintering. After laser sintering, the adhesion force between the TiO_2 film and the flexible substrate is still good (see the video in the supporting information).

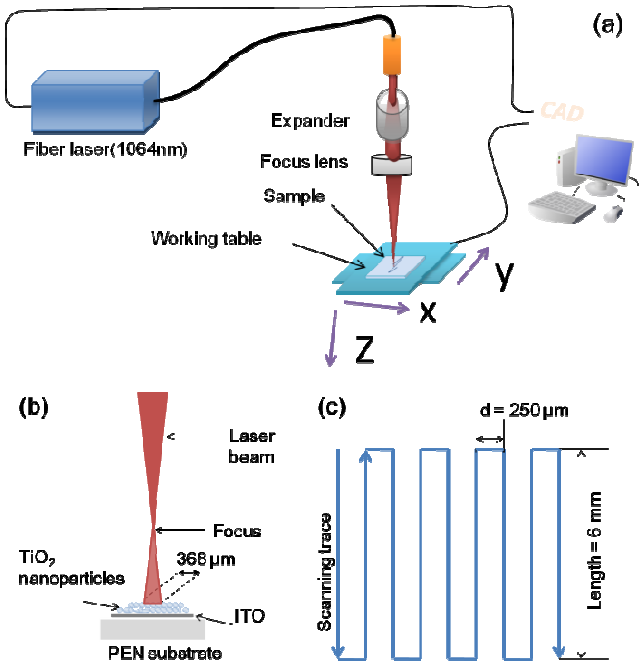

Fig. 1 Schematic show of (a) the computer controlled automatic laser sintering system; (b) the irradiation way of laser beam on TiO_2 film: the focus was set 14 mm above the film, with the circular spot diameter of 368 μm reaching the film surface; and (c) the scanning trace of laser beam on TiO_2 film.

For solar cell fabrication, the TiO_2 films were then soaked in 0.5 mM N719 dye solution in the mixture of tert-butanol and acetonitrile (1: 1, by volume) for 18 h at room temperature. The dyed films were then sealed with the platinized counter electrodes by using Surlyn films (25 μm, DuPont) as the spacers. The sandwich type solar cells were completed by filling of liquid electrolyte through the drilled holes. The electrolyte consists of 1.0 M 1,3-dimethylimidazolium iodide, 50 mM LiI, 30 mM I_2, 0.5 M tert-butylpyridine, and 0.1 M guanidinium thiocyanate in the mixed solvent of acetonitrile and valeronitrile (85: 15, by volume).

Characterizations

The morphology of TiO_2 films has been examined by using scanning electron microscope (SEM, FEI-Sirion 200, FEI) and scanning probe microscopy (SPM, Nanoscope Multimode/Dimension, Digital Instruments Inc.). The film thickness was determined by a Veeco Dektak 150 surface profiler. The Raman spectroscopy was carried out with a WITec confocal Raman microscope (alpha 300R).[28] The excitation source is a 532 nm laser (2.33 eV) with a laser power below 0.1mW on the sample to avoid laser-induced local heating. The laser spot size at focus was around 500 nm in diameter with a 100× objective lens (NA = 0.95). The spectral resolution is 1 cm^{-1}.

The solar cell performances were evaluated using a solar simulator (100 mW cm^{-2}, the equivalent of one sun at AM1.5G).A 450 W xenon light source solar simulator (Oriel, model 9119) with AM 1.5G filter (Oriel, model 91192) was used to give an irradiance of 100 mW cm^{-2} at the surface of the solar cell. The current-voltage characteristics of the cell under these conditions were obtained by applying external potential bias to the cell and measuring the generated photocurrent with a Keithley

model 2400 digital source meter (Keithley, USA). A similar data acquisition system was used to control the IPCE measurement. A white light bias (1% sunlight intensity) was applied onto the sample during the IPCE measurements with ac model (10 Hz). The active area for solar cell testing determined by the square mask is 4× 4 mm^2.

Electrochemical impedance spectroscopy (EIS) measurements were measured using the PGSTAT302N frequency analyzer from Autolab (Eco Chemie B.V, Utrecht, The Netherlands) together with the Frequency Response Analyzer module providing voltage modulation in the desired frequency range. The Z-view software (v2.8b, Scribner Associates Inc.) was used to analyze the impedance data. The EIS experiments were performed at a constant temperature of 25 °C in the dark. The impedance spectra of the series devices were recorded at potentials varying from -0.4 V to -0.8 V at frequencies ranging from 0.01 Hz to 200 KHz, the oscillation potential amplitudes being adjusted to 10 mV.

For the transient photovoltage/photocurrent decays measurements,[29, 30] a white light bias on the DSC sample was generated from an array of diodes. Red light pulse diodes (0.05 s square pulse width, 100 ns rise and fall time) controlled by a fast solid-state switch were used as the perturbation source. The voltage dynamics were recorded on a PC-interfaced Keithley 2602A source meter with a 100 μs response time. The perturbation light source was set to a suitably low level in order for the voltage decay kinetics to be monoexponential. By varying the white light bias intensity, the recombination rate constant and electron diffusion rate constant could be estimated over a range of applied biases.

Results and Discussion

At the laser sintering conditions, it was found the TiO_2 film could be effectively sintered which will be described in later sections, whilst the ITO/PEN plastic substrate could keep unchanged on sheet resistance and optical transparency before and after laser sintering (Figure S1). The selectivity of sintering effect on the TiO_2 film and the ITO/PEN substrate is suggested to arise from different light absorption of each layer (Figure S2). The TiO_2 layer rather than the ITO and PEN layers absorbs the main part of the laser energy, and as a result, the highest temperature rise should occur in such a TiO_2 layer. Besides, the choice on the laser wavelength of 1064 nm is found important for the sintering effect of the TiO_2 film. For a similar laser sintering setup but with a UV laser source (355 nm), it was found that the laser energy was only strongly absorbed within an ultrathin (100-200 nm) top-layer of the TiO_2 film, as a result of which a heavily melted dense top-layer was formed (Figure S3). Such a layer capping the nanoparticles under-layer would block electrolyte diffusion and therefore hinder the solar cell performance. In a pointy contrast, the near IR laser has higher optical penetration length in the TiO_2 film which can result in more homogenous and mild sintering effect across the whole film depth. That is because the near-infrared light absorption by the TiO_2 film, associated with intra band-gap energy levels related to oxygen vacancies,[31] is relatively weak in comparison to indirect inter-band photon absorption of UV light.

Figure 2a shows a cold isostatic pressed TiO_2 film on ITO/PEN flexible substrate. It is optically semi-transparent, reflecting the densely packing of nanoparticles after compression.[22, 23] Inside the film, there are three laser sintered patterns denoted by the red arrows (square, circle and triangle, from left to right). These patterns which are observed more opaque can be clearly identified from the base film. The general thinking at this point is: could it be the change on film morphology leading to such optical difference between the laser sintered regions and the base film. However, when we carefully checked both regions by SEM and SPM (Figure 2b, c), no microstructure difference could be detected. The SPM tested mean roughnesses are 9.597 nm and 10.371 nm before and after laser sintering. Therefore, we strongly suspect there should be other reasons responsible for the optical change.

We then turned to Raman micro-spectroscopy to characterize the laser sintering effect on the TiO_2 (P25) film. The results are shown in Figure 3. It is known that P25 nanoparticles consist of roughly about 80% anatase and 20% rutile phase.[32] That is confirmed in Figure 3a, for the unsintered film, the peaks at 144, 197, 399, 515, 519 (superimposed with the 515 cm^{-1} band), and 639 cm^{-1} owing to anatase phase dominate the Raman spectrum. Those peaks can be attributed to the six Raman-active modes of anatase phase with the symmetries of E_g, E_g, B_{1g}, A_{1g}, B_{1g}, and E_g, respectively.[33] The Raman peaks owing to rutile phase at 235 cm^{-1}, 445 cm^{-1} and 612 cm^{-1}, which correspond to two-phonon scattering, E_g, and A_{1g} modes respectively.[33] Those peaks are very weak in the unsintered film, which, however, rise evidently after laser sintering. The result strongly suggests the increase of rutile phase in the laser sintered film. That is to say, undergoing laser sintering, a considerable fraction of anatase phase in the P25 film is transformed into rutile phase. The Raman mapping on the interface between the sintered and unsintered regions clearly show this point. Figure 3c shows the Raman mapping results, of which the detective area corresponds to the same red square region in Figure 3b. From the optical micrograph of Figure 3b, a clear interface between the left sintered region and the right unsintered region can be clearly found in the middle, according to their obvious brightness contrast. From Figure 3c, such interface could also be identified according to the contrasts of the

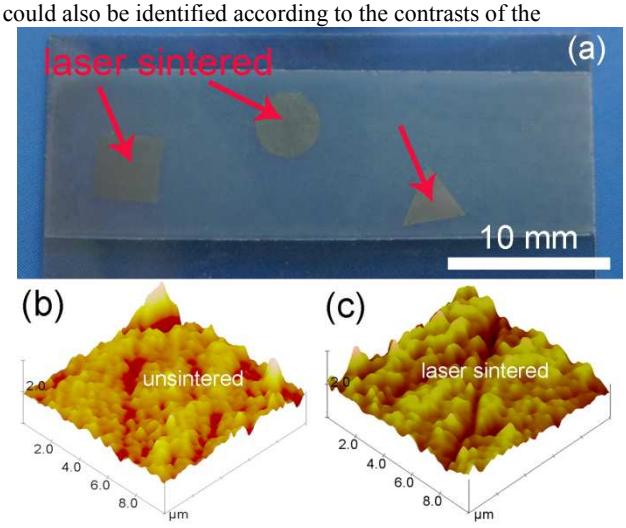

Fig. 2 (a) optical image of the cold isostatic pressed TiO_2 film on ITO-PEN substrate including three laser sintered patterns, from left to right are square, circle and triangle which are labeled by the red arrows; SPM images of different regions of the TiO_2 film: (b) before and (c) after laser sintering.

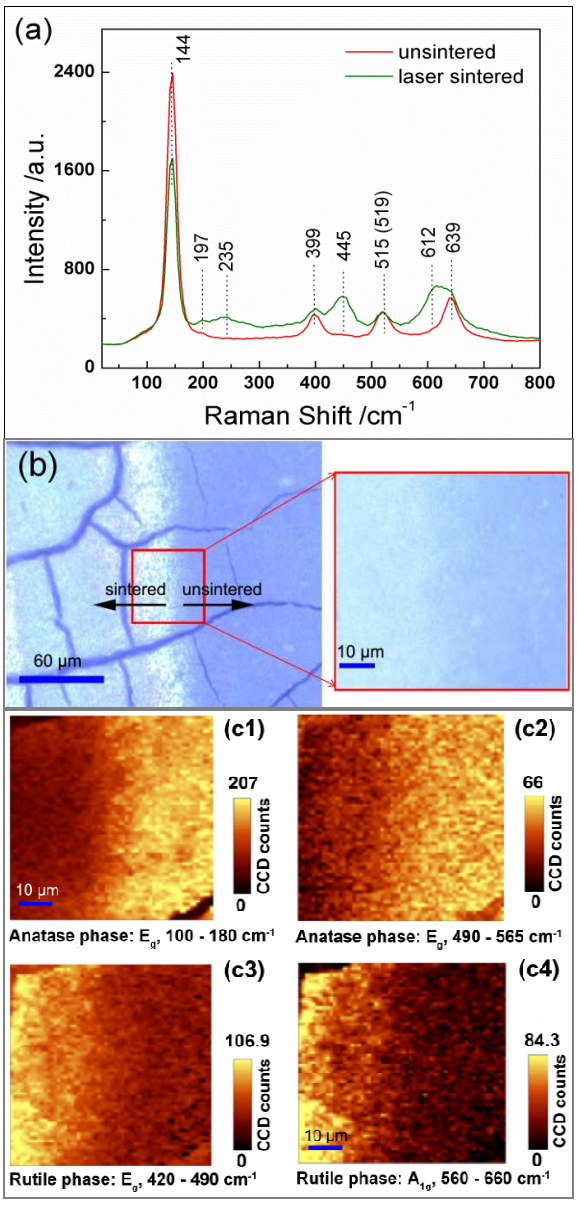

Fig. 3 (a) Raman spectra of the laser sintered and unsintered TiO_2 (P25) films; (b) optical micrograph showing the detective area of Raman mapping on the TiO_2 film (highlighted by the red square), including the interface of the laser sintered (in the left) and unsintered (in the right) regions, the scale bar XX; (c1-c4) Raman maps of the same region in (b), describing the contrasts on the integrated intensities of Raman signals in the ranges of 100 -180 cm^{-1} (c1), 490 – 565 cm^{-1} (c2), mainly attributed to the anatase phase, and 420 – 490 cm^{-1} (c3), 560 – 660 cm^{-1} (c4), mainly attributed to the rutile phase. Note that the TiO_2 film in (b) is without compression.

integrated intensities of Raman signals between the laser sintered and unsintered regions. The Raman signals owing to anatase phase (100-180 cm^{-1} and 490-565 cm^{-1}) in the left sintered region are much higher than the right unsintered region; while the Raman signals owing to rutile phase (420-490 cm^{-1} and 560-660 cm^{-1}) are just on the contrary. All of these results show that more rutile phase and less anatase phase are included in the sintered region than the unsintered one, which consistently demonstrate the laser sintering induced phase transition from anatase to rutile.

Such phase transition is known to occur only at the temperature of higher than 550 °C by conventional furnace sintering for hours. However, it was realized within seconds by the near-IR laser sintering. Indeed, the laser scanning mode at the current state is "point to line", it is not appropriate to treat a very large film. However, it is feasible to improve the scanning mode to "line to plane" as schematically shown in Figure S4 by replacing the point laser source to be a line laser,[34] the selective laser sintering will be scalable and of great possibility to be integrated into the non-stop roll-to-roll production line. Besides, such fast phase transition did not accompany with crystal size growth, which was generally involved in conventional furnace sintering.[35] Therefore, the high dye loading content of the P25 film could be maintained before and after laser sintering, which was tested to be 1.33×10^{-7} and 1.25×10^{-7} mol cm^{-2} respectively. High speed and no evident change on film morphology are outstanding advantages for the selective laser sintering raised in this work.

Furthermore, from the above Raman analysis, the as-demonstrated phase transition may just explain the inherent cause for the optical difference between the laser sintered regions and the base film (Figure 2a). As we known, rutile TiO_2 in comparison anatase has higher refractive index,[36] meaning higher light scattering ability, which generally make it look whiter and has been applied as a scattering layer in DSCs extensively.[37, 38] Since higher content of rutile phase are contained in the laser sintered regions, it is understandable such regions look more opaque in Figure 2a. Indeed, the stronger light scattering of the laser sintered film than the unsintered one has also been confirmed by their diffuse reflectance spectra (Figure S5).

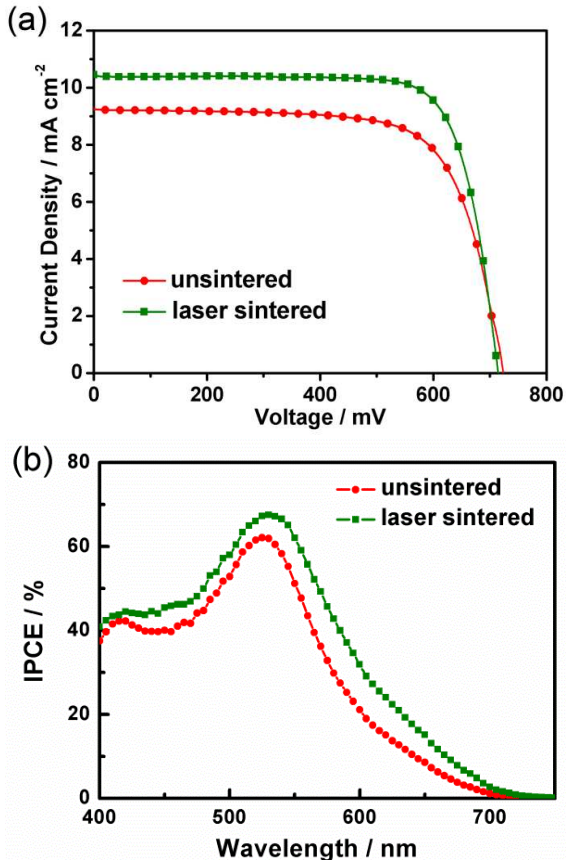

Fig.4 (a) Current density-voltage characteristic curves and (b) IPCE spectra of the two compared flexible solar cells based on the laser sintered and unsintered TiO_2 films.

Table 1 The performance of flexible DSCs based on the TiO_2 film before and after laser sintering

Samples	V_{oc} / mV	J_{sc} / mA cm^{-2}	Fill factor	Efficiency
Unsintered	720	9.2	0.71	4.6%
Laser sintered	716	10.4	0.77	5.7%

Figure 4a shows the current density-voltage characteristic curves of flexible DSCs made of TiO_2 nanoparticles films with and without laser sintering. The performance parameters are summarized in Table 1. It could be clearly found that the short-circuit current density (J_{sc}) is evidently increased from 9.2 to 10.4 mA cm^{-2} associated with laser sintering. Besides, fill factor is also increased dramatically from 0.71 to 0.77. These two improvements lead to the overall efficiency be increased dramatically by 23.9%, from 4.6% to 5.7% under 1 sun illumination. For flexible DSCs based on Degussa P25 TiO_2 nanoparticles, the efficiency of 5.7% in this work is comparable to the top-level records reported previously,[22, 39-42] given that the light scattering layer, dense under layer, etc. have been ignored. This highlights the positive effect of the selective laser sintering. Figure 4b presents the IPCE spectra of the two compared solar cells. By integration of the IPCE curves could explain the two samples' J_{sc} difference.

In order to clarify the inherent causes for laser sintering induced performance enhancement, we performed EIS measurements under dark condition on the two compared solar cells. The important elements, including interfacial recombination resistance (R_{ct}), electron transport resistance (R_t), and electron diffusion length (L) were extracted from fitting the impedance data by the transmission line model.[43] Figure 5a shows the dependences of R_{ct} on the dark current and Figure 5b shows the dependences of R_t on the energy difference between the quasi-Femi level of TiO_2 and the redox potential of electrolyte ("$E_{Fn} - E_{redox}$"). As presented in Figure 5a and 5b, associated with laser sintering, the recombination resistance becomes larger, which means the back electron transfer through the TiO_2/electrolyte interface is largely reduced; while the electron transfer resistance becomes smaller. Correspondingly, the effective electron diffusion length, defined as $L = d \times (R_{ct}/R_t)^{1/2}$,[44] is increased for the sample with laser sintering (Figure 5c). Besides, it is known that R_t will contribute to the total series resistance of DSC and R_{ct} will contribute to the shunt resistance. According to the one-diode model for solar cells, the decrease of series resistance and the increase of shunt resistance will both benefit for rectifying effect, leading to the increase of fill factor of solar cells.[45] Therefore, it is understandable for the laser sintered sample got notably higher fill factor than the unsintered one (Table 1).

Figure 6 shows the results obtained from transient photovotage/photocurrent decays measurements. As shown in Figure 6a, the electron diffusion coefficient (D_e) is enhanced after laser sintering, which is consistent with the decreased electron transfer resistance in Figure 5b.[46] The apparent electron lifetime (τ_n) as function of irradiating light intensity is plotted in Figure 6b. Obviously, the lifetime between the electrons in the TiO_2 conduction band and oxidized state component of electrolyte is longer after laser sintering. This result is in consistent with the increased recombination resistance in Figure 5a. Thus, the enhanced charge collection efficiency (η_{cc}, Figure 6c) is found for

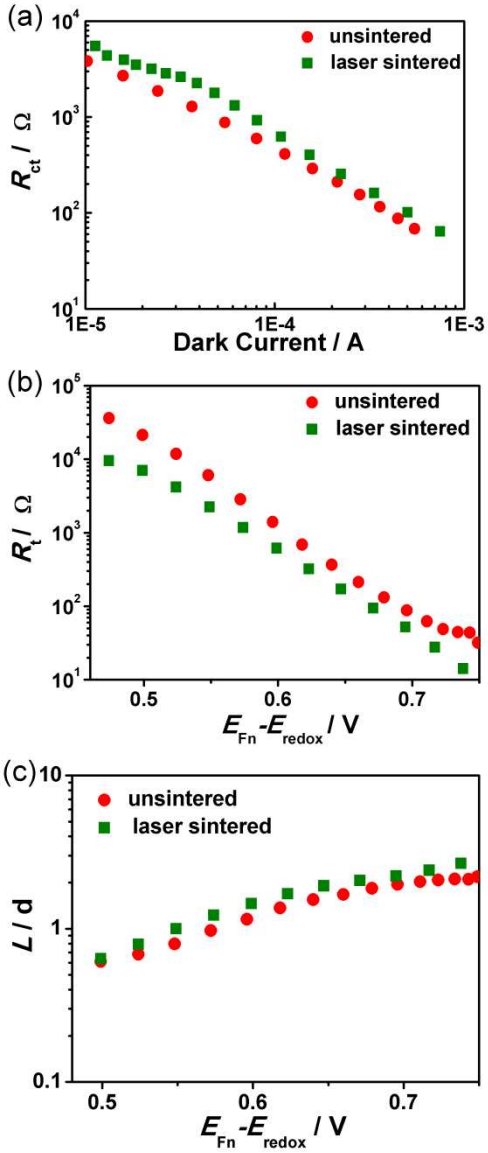

Fig.5 (a) the interfacial recombination resistance R_{ct} (b) the electron transport resistance R_t, and c) the ratio between electron diffusion length (L) and actual film thickness (d) obtained from impedance measurements in dark (corrected for the iR drop due to series resistance).

the sample with laser sintering, which is in consistent with the increased electron diffusion length in Figure 5c. The improvement in η_{cc} could be mostly responsible for the IPCE improvement in Figure 4b. The relative increase in η_{cc} is about only 2-4% in average, which cannot explain the total increase of IPCE (by 5-8%) especially in the 600-700 nm wavelength range. Such mismatch might be compensated by the light scattering enhancement in the laser sintered film with higher rutile phase content.

At the end, a key question raised is: why laser sintering could result in such changes on the electrochemical elements, kinetic parameters of the solar cell devices, as described in Figure 5 and 6. From the view point of materials science, it might be answered as follows. First, the laser sintering may simultaneously induce inter-nanoparticles neck formation during the quick phase transition from anatase to rutile, which will result in more fluent

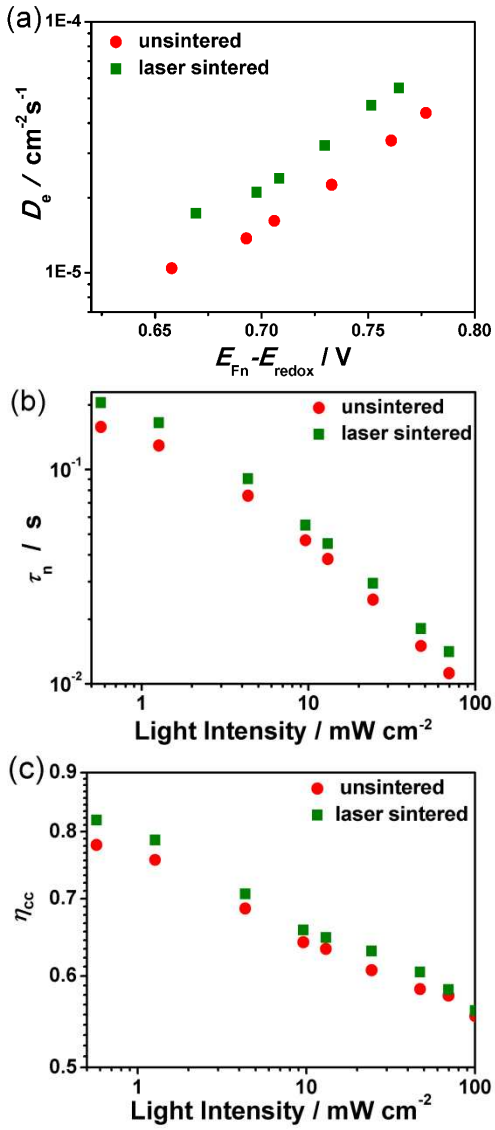

Fig.6 The results obtained from photovoltage/ photocurrent decays measurements: (a) the electron diffusion coefficient (D_e) as function of open-circuit potential, (b) apparent recombination lifetime (τ_n), and (c) charge collection efficiency (η_{cc}) as function of light intensity.

electron transfer paths and decreased electron transfer resistance.[47-50] Second, the temperature rise effect of the laser sintering might result in cleaner surfaces of TiO_2 nanoparticles due to remove of some unwanted adsorbents or dangling bonds, and therefore largely retard the interfacial recombination kinetics of the solar cell device.[51-54]

Conclusion

In summary, we have first demonstrated the validity of a facile selective laser sintering technique on the fabrication of TiO_2 nanoparticles film on conductive plastic substrate for highly efficient flexible DSC application. The laser sintering effects are reflected in the following aspects: (1) the sintering induced partial crystal phase transition from anatase to rutile while keeping the film morphology nearly unchanged; (2) the optical property change: light scattering of the laser sintered TiO_2 film is enhanced; (3) no damage to the plastic conductive substrate. The EIS and photovoltage/photocurrent decays characterizations have consistently demonstrated the positive effect of laser sintering on charge collection of the solar cell, by both reducing the electron transport resistance and increasing the interfacial recombination resistance. IPCE and J_{sc} are accordingly increased. Another associated benefit is much increased fill factor. Taking together, flexible DSC after laser sintering has achieved improved efficiency of 5.7%, which is 23.9% higher than the unsintered sample. Noteworthy is that the laser treatment is a fast process: the effective sintering time is dramatically decreased from hours in a conventional furnace to seconds. It is of great potential for this technique to be integrated into scalable roll-to-roll manufacture of highly efficient flexible DSC in the future.

Acknowledgement

This work was supported by the National Natural Science Foundation (21103058, 21173091, 20903030), 973 Program of China (2011CBA00703), Natural Science Foundation of Hubei Province (2011CDB033, 2011CDB0.4) and Basic Scientific Research Funds for Central Colleges (2012YQ027, 2013TS040). We also thank Analytical and Testing Center of Huazhong University Science & Technology for the sample measurements. Prof. Q. Bao acknowledges the support from ARC DECRA and MCN Technology Fellowship/ANFF-Victoria.

Notes and references

[a] *Michael Grätzel Centre for Mesoscopic Solar Cells, Wuhan National Laboratory for Optoelectronics and College of Optoelectronic Science and Engineering, Huazhong University of Science and Technology, Wuhan 430074, P. R. China. Fax: 86 8779 3867; Tel: 86 8779 3867; E-mail: wnlochenwei@hust.edu.cn (Prof. W. Chen); mingkuiwang@hust.edu.cn (Prof. M. Wang); duans@hust.edu.cn (Prof. J. Duan)*

[b] *Department of* Materials Engineering, Monash University, Melbourne, Victoria, 3800, Australia

[c] *Department of Chemistry, The Hong Kong University of Science and Technology, Clear Water Bay, Kowloon, Hong Kong*

[†] These authors contributed equally to this work.

† Electronic Supplementary Information (ESI) available: [a video demonstration of good adhesion between TiO_2 film and flexible substrate, laser sintering effect on ITO/PEN film, optical difference of difference layer, different sintering effect on TiO_2 film by different laser sources, proposed sintering mode by line laser source, and diffuse reflectance of TiO_2 films]. See DOI: 10.1039/b000000x/

References

1 M. Pagliaro, R. Ciriminna, G. Palmisano, *ChemSusChem*, 2008, **1**, 880.

2 R. Søndergaard, M. Hösel, D. Angmo, T. T. Larsen-Olsen, F. C. Krebs, *Mater. Today*, 2012, **15**, 36.

3 D. Shahrjerdi, S. W. Bedell, C. Bayram, C. C. Lubguban, K. Fogel, P. Lauro, J. A. Ott, M. Hopstaken, M. Gayness, D. Sadana, *Adv. Energy Mater*., 2013, **3**, 542.

4 A. Chirila, P. Bloesch, S. Seyrling, A. Uhl, S. Buecheler, F. Pianezzi, C. Fella, J. Perrenoud, L. Kranz, R. Verma, D. Guettler, S. Nishiwaki, Y. E. Romanyuk, G. Bilger, D. Brémaud, A.N. Tiwari, *Prog. Photovolt: Res. Appl.*, 2011, **19**, 560.

5 S. F. Zhang, X. D. Yang, Y. H. Numata, L. Y. Han, *Energy Environ. Sci.*, 2013, **6**, 1443.

6 K. Miettunen, J. Halme, P. Lund, *WIREs Energy Environ.*, 2013, **2**, 104.

7 S. K. Balasingam, M. G. Kang, Y. Jun, *Chem. Commun.*, 2013, **49**, 11457.

8 Y. Fu, Z. Lv, S. Hou, H. Wu, D. Wang, C. Zhang, D. Zou, Adv. Energy Mater, 2012, 2, 37.

9 J. Liao , B. Lei , H. Chen , D. Kuang, C. Su, *Energy Environ. Sci.*, 2012, **5**, 5750.

10 J. Wu, Y. Xiao, Q. Tang, G. Yue, J. Lin, M. Huang, Y. Huang, L. Fan, Z. Lan, S. Yin, T. Sato, *Adv. Mater.*, 2012, **24**, 1884.

11 F. Yang, K. Cheng, Y. Mo, L. Yu, J. Yin, G. Wang, D. Cao, *J. Power Sources*, 2012, **208**, 197.

12 T. Yamaguchi, N. Tobe, D. Matsumoto, T. Nagai, H. Arakawa, *Sol. Energy Mater. Sol. Cells*, 2010, **94**, 812.

13 A. Yella, H. W. Lee, H. N. Tsao, C. Y. Yi, A. K. Chandiran, *Science*, 2011, **334**, 629.

14 S. Nakade, M. Matsuda, S. Kambe, Y. Saito, T. Kitamura, T. Sakata, Y. Wada, H. Mori, S. Yanagida, *J. Phys. Chem. B*, 2002, **106**, 10004.

15 D. S. Zhang, J. A. Downing, F. J. Knorr, J. L. McHale, *J. Phys. Chem. B*, 2006**, 110**, 21890.

16 G. Boschloo, H. Lindström, E. Magnusson, A. Holmberg, A. Hagfeldt, *J. Photochem. Photobiol. A: Chem.*, 2002, **148**, 11.

17 D. S. Zhang, T. Yoshida, T. Oekermann, K. Furuta, H. Minoura, *Adv. Funct. Mater.* , 2006, **16**, 1228.

18 S. Uchida, M. Tomiha, H. Takizawa, M. Kawaraya, *J. Photochem. Photobiol., A* , 2004, **164** , 93.

19 N.-G. Park, K.□M. Kim, M.□G. Kang, K.□S. Ryu, S.□H. Chang, Y.-J. Shin, *Adv. Mater.*, 2005, **17**, 2349.

20 W. Chen, Y. Qiu, S. Yang, *Phys. Chem. Chem. Phys.*, 2010, **12**, 9494.

21 M. Dürr, A. Schmid, M. Obermaier, S. Rosselli, A. Yasuda, G. Nelles, *Nature Materials*, 2005, **4**, 607.

22 Y. Peng, J. Z. Liu, K. Wang, Y.-B. Cheng, *Int. J. Photoenergy*, 2011, **2011**, 7.

23 H. C. Weerasinghe, P. M. Sirimanne, G. P. Simon, Y.-B. Cheng, *Prog. Photovolt: Res. Appl.*, 2012, **20**, 321.

24 J. Kim, J. Kim, M. Lee, *Nanotechnology*, 2010, **21**, 345203.

25 G. Mincuzzi, M. S. Ruhtenberg, L. Vesce, A. Reale, A. D. Carlo1, A. Gillner, T. M. Brown, *Prog. Photovolt: Res. Appl.*, 2012, DOI: 10.1002/pip.2261.

26 G. Mincuzzi, L. Vesce, A. Reale, A. D. Carlo, T. M. Brown, *Appl. Phys. Lett.*, 2009, **95**, 103312.

27 M. J. Carnie, C. Charbonneau, P. R. F. Barnes, M. L. Davies, I. Mabbett, T. M. Watson, B. C. O'Regan, D. A. Worsley, *J. Mater. Chem. A*, 2013, **1**, 2225.

28 M. Jaiswal , C. H. Y. X. Lim ,Q. L. Bao, C. T. Toh, K. P. Loh, B. Özyilmaz, *ACS Nano*, 2011, **5**, 888.

29 D. Xiong, W. Zhang, X. Zeng, Z. Xu, W. Chen, J. Cui, M. Wang, L. Sun, Y.-B. Cheng, *ChemSusChem*, 2013, **6**, 1432.

30 X. Xu, B. Zhang, J. Cui, D. Xiong, Y. Shen, W. Chen, L. Sun, Y.-B. Cheng and M. Wang, *Nanoscale*, 2013, **5**, 7963.

31 Y. Nakano, T. Morikawa, T. Ohwaki, Y. Taga, *Chem. Phys.*, 2007, **339**, 20.

32 M. C. Yan, F. Chen, J. L. Zhang, M. Anpo, *J. Phys. Chem. B*, 2005, **109**, 8673.

33 J. Zhang, M. J. Li, Z. C. Feng, J. Chen, C. Li, *J. Phys. Chem. B*, 2006, **110**, 927.

34 L. M. Dong, J. Li, C. Y. Ni, Z. H. Shen, X. W. Ni, *Int. J. Thermophys.*, 2013, **34**, 1066.

35 A. Nakaruk, D. Ragazzon, C.C. Sorrell, *Thin Solid Films*, 2010, **518**, 3735.

36 Q. Gao, X. M. Wu, Y. M. Fan, X. Y. Zhou, *Dyes and Pigments*, 2012, **95**, 534.

37 Z. Lan, J. H. Wu, J. M. Lin, M. L. Huang, *J. Inorg. Mater.*, 2011, **26**, 119.

38 H. Wang, M. Miyauchi, Y. Ishikawa, A. Pyatenko, N. Koshizaki, Y. Li, L. Li, X. Li, Y. Bando, D. Golberg, *J. Am. Chem. Soc.*, 2011, **133**, 19102.

39 S. Senthilarasu, T. A. N. Peiris, J. G. Cañadas, K. G. U. Wijayantha , *J. Phys. Chem. C*, 2012, **116**, 19053.

40 G. Hashmi, K. Miettunen, T. Peltola, J. Halme, I. Asghar, K. Aitola, M. Toivola, P. Lund, *Renew. Sust. Energ. Rev.*, 2011, **15**, 3717.

41 H. Lee, D. Hwang, S. M. Jo, D. Kim, Y. Seo, D. Y. Kim, *ACS Appl. Mater. Interfaces*, 2012, **4**, 3308.

42 X. Yin, Z. S. Xue, L. Wang, Y. M. Cheng, B. Liu, *ACS Appl. Mater. Interfaces*, 2012, **4**, 1709.

43 J. Bisquert, G. G. Belmonte, F. F. Santiago, N. S. Ferriols, P. Bogdanoff, E. C. Pereira, *J. Phys. Chem. B*, 2000, **104**, 2287

44 M. A. Hossain, J. R. Jennings, N. Mathewsb, Q. Wang, *Phys. Chem. Chem. Phys*., 2012, **14**, 7154.

45 Q. Wang, S. Ito, M. Grätzel, F. F. Santiago, I. M. Seró, J. Bisquert, T. Bessho, H. Imai, *J. Phys. Chem. B*, 2006, **110**, 25210.

46 M. K. Wang, P. Chen, R. H. Baker, S. M. Zakeeruddin, M. Grätzel, *Chem. Phys. Chem.*, 2009, **10**, 290.

47 A. J. Frank, N. Kopidakis, J. V. D. Lagemaat, *Coord. Chem. Rev.*, 2004, **248**, 1165.

48 K. D. Benkstein, N. Kopidakis, J. V. D. Lagemaat, A. J. Frank, *J. Phys. Chem. B*, 2003, **107**, 7759.

49 W. Chen, Y. Qiu, S. Yang, *Phys. Chem. Chem. Phys.*, 2012, **14**, 10872.

50 W. Chen, Y. Qiu, Y. Zhong, K. S. Wong, S. Yang, *J. Phys. Chem. A*, 2010, **114**, 312.

51 N. Kopidakis, N. R. Neale, K. Zhu, J. V. Lagemaat, A. J. Frank, *Appl. Phys. Lett.*, 2005, **87**, 202106.

52 J. V. D Lagemaat, A. J. Frank, *J. Phys. Chem. B*, 2000, **104**, 4292.

53 D. Kim, A. Ghicov, S. P. Albu, P. Schmuki, *J. Am. Chem. Soc.*, 2008, **130**, 16454.

54 J. Bisquert, A. Zaban, P. Salvador, *J. Phys. Chem. B*, 2002, **106**, 8774.

A table of contents entry:

Colour graphic: maximum size 8 cm x 4 cm

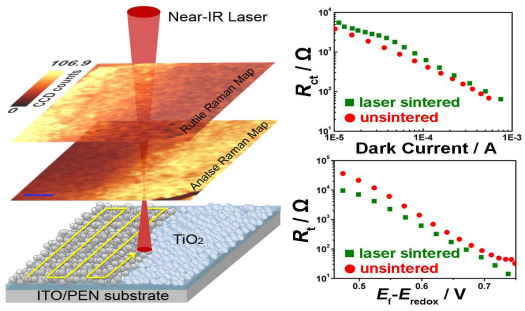

Text: one sentence, of maximum 20 words, highlighting the novelty of the work

Fast and selective laser sintering has been demonstrated efficient on the treatment of TiO_2 nanoparticles film for flexible DSSC application.